RMP Colloquia

Spin-exchange optical pumping of noble-gas nuclei

Thad G. Walker

Department of Physics, University of Wisconsin-Madison, Madison, Wisconsin 53706

William Happer

Department of Physics, Princeton University, Princeton, New Jersey 08544

Spin-exchange optical pumping of mixtures of alkali-metal vapors and noble gases can be used to efficiently polarize the nuclei of the noble-gas atoms. Liters of noble gases at standard temperature and pressure and with nuclear spin polarizations of several tens of percent are now used in many applications. The authors describe the basic phenomena that govern the spin-exchange process and review the physics of angular momentum transfer and loss in optical pumping and spin-exchange collisions. [S0034-6861(97)00802-7]

CONTENTS

I. INTRODUCTION

In spin-exchange optical pumping, circularly polarized resonance light is absorbed by a saturated vapor of alkali-metal atoms contained in a glass cell. The cell also includes a much larger quantity of noble-gas atoms. In well-designed systems, nearly half of the spin angular momentum of the absorbed photons is transferred to the alkali-metal atoms, thereby spin-polarizing the valence electrons of the alkali-metal atoms. Subsequent collisions between the alkali-metal atoms and noble gas atoms transfer some of the electron-spin polarization to the nuclei of the noble gas.

Many applications use spin-exchange optical pumping for producing large numbers of spin-polarized nuclei. Some examples are the first determination of the neutron spin-structure function, measured by scattering polarized, high-energy electrons from highly polarized targets of ^{3}He (Anthony *et al.*, 1993); magnetic resonance imaging of lungs and other organs of the human body with the gases ^{3}He and ^{129}Xe (Albert *et al.*, 1994; Middleton *et al.*, 1995); studies of surface interactions (Wu *et al.*, 1990; Raftery *et al.*, 1991); studies of fundamental symmetries (Newbury *et al.*, 1991; Chupp *et al.*, 1994); neutron polarizers and polarimeters (Thompson *et al.*, 1992). Recently developed high-power diode-laser arrays, which can provide tens to hundreds of watts of pumping light, have greatly decreased the cost and improved the performance of spin-exchange optical pumping, and so its use seems likely to grow. An *in vivo* image of a human lung, obtained using ^{3}He gas that was polarized by spin-exchange optical pumping, is shown in Fig. 1.

Laser technology is progressing so rapidly that the details of spin-exchange optical pumping systems are continually changing. Familiarity with the basic physics of spin-exchange optical pumping will make the exploitation of new technology much more efficient, and one goal of this colloquium is to provide a convenient summary of the current state of knowledge. We shall also point out important gaps in our understanding and areas where further research would have important payoffs. After a brief overview in Sec. II, the interchange of angular momentum between a light beam and alkali-metal atoms is discussed in Sec. III. The interchange of spin between alkali-metal atoms and the nuclei of noble-gas atoms is discussed in Sec. IV. The fundamental origin of the spin-dependent interactions between alkali-metal atoms and noble-gas atoms is discussed in Sec. V. Since

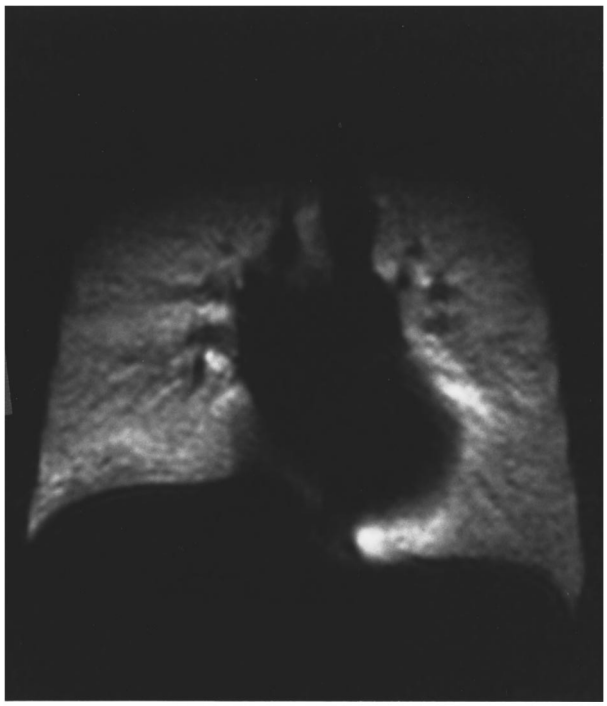

FIG. 1. Image of a human lung using spin-exchange-polarized ^{3}He (MacFall *et al.*, 1996).

the physics of these interactions is subtle, Sec. V is rather detailed. The most important parasitic spin-loss mechanisms of alkali-metal atoms and noble-gas atoms are discussed in Sec. VI.

II. OVERVIEW OF SPIN-EXCHANGE OPTICAL PUMPING

Figure 2 shows a typical experimental arrangement for spin-exchange optical pumping. A glass cell of a few cm^3 volume, carefully prepared to remove paramagnetic impurities from the walls (Newbury, Barton, Cates, Happer, and Middleton, 1993), contains the gases of interest, namely, alkali-metal vapor and a noble gas, plus

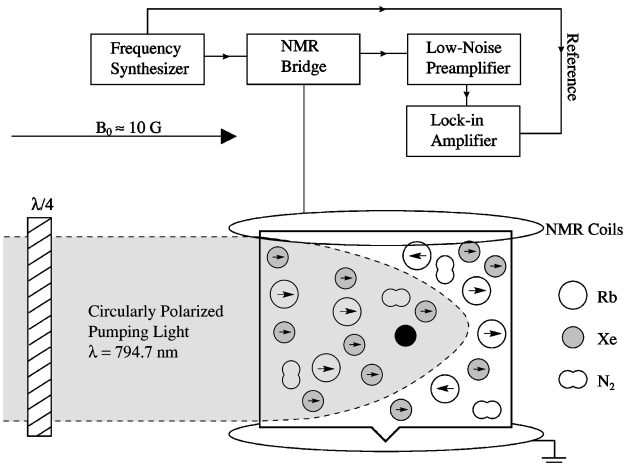

FIG. 2. Experimental arrangement for spin-exchange optical pumping.

nitrogen. Although any of the alkali metals are suitable, rubidium is often chosen. The high vapor pressure of rubidium allows operation at modest temperatures where chemical attack on the glass container is not a problem. The 7947 Å resonance line lies in a region of the spectrum where intense, tunable light sources such as dye lasers, titanium sapphire lasers, and gallium aluminum arsenide injection lasers exist. A simple oven keeps the cell at a constant temperature, usually in the range between 80 °C and 130 °C. This ensures an adequate saturated vapor pressure (typically 10^{11} to 10^{14} cm^{-3}) from a few droplets of Rb metal in the cell. A few to many tens of watts of circularly polarized laser light spin-polarizes the alkali-metal atoms via optical pumping. The nitrogen, which is chemically inert, suppresses reradiation of light by quenching the excited atoms. The pressure of the noble gas which is to be polarized by spin-exchange is usually in the range of 10 Torr to 10 atmospheres. During binary collisions, the hyperfine interaction between the alkali-metal electron and the noble-gas nucleus partially transfers spin polarization from the alkali-metal atoms to the noble-gas atoms. Repeated collisions increase the nuclear-spin polarization to several tens of percent, typically five orders of magnitude larger than the thermal polarization obtainable in even the largest laboratory magnetic fields.

The buildup of the nuclear polarization of the noble gas is most conveniently monitored by nuclear magnetic resonance (NMR). The nuclear polarization is so large that almost any continuous or pulsed NMR method will work. Indeed, masing of the highly polarized spins can easily occur if high-Q NMR coils are used (Chupp *et al.*, 1994). The polarization can be absolutely calibrated by comparison with the NMR signal from a water sample in a cell with the same shape (Bhaskar *et al.*, 1982). One can also measure the absolute noble-gas nuclear polarization by observing the resulting shift of the electron-paramagnetic-resonance (EPR) frequencies of the alkali-metal atoms (Newbury, Barton, Bogorad, *et al.*, 1993). The EPR shifts result from the hyperfine interaction and are typically a few kilohertz for situations of practical interest. As is well known, frequency measurements can be relatively free of systematic errors. It is also possible to monitor optically the small electron-spin polarization induced in a non-optically-pumped alkali-metal vapor by the nuclear-spin polarization of the noble gas (Bhaskar *et al.*, 1983; Zeng *et al.*, 1983).

III. OPTICAL PUMPING

A. Interaction of alkali-metal atoms with circularly polarized light

Optical pumping uses light to spin-polarize both the electron spin S and the nuclear spin I_a of the alkali-metal atoms[1] (Happer, 1972). The atoms are subject to a

[1]Here and later, the subscripts a and b refer to alkali-metal and noble-gas atoms, respectively.

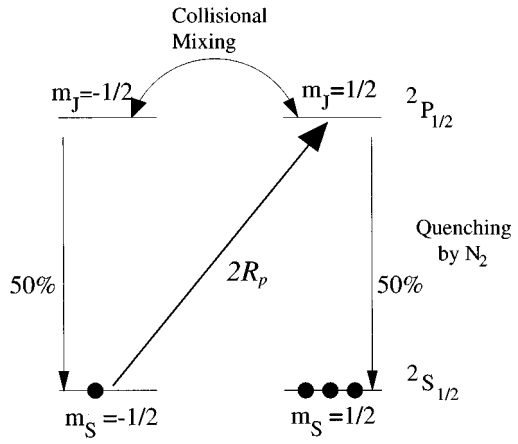

FIG. 3. The interaction of alkali-metal atoms with left-circularly (σ^+) polarized light.

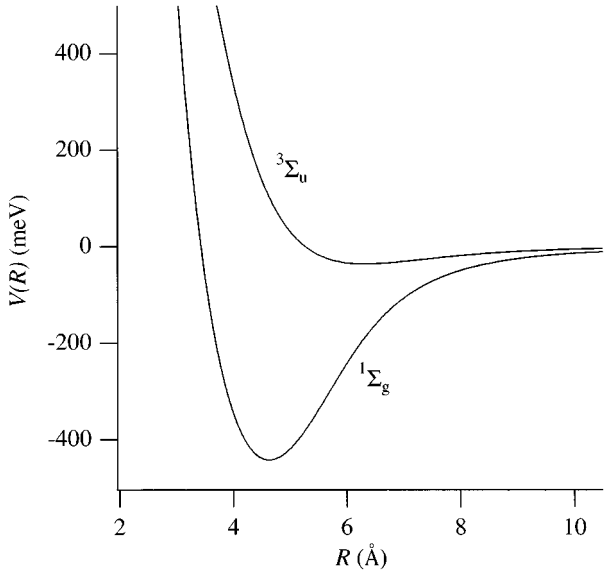

FIG. 4. Singlet and triplet potential energies as a function of the internuclear separation R between a pair of cesium atoms (Krauss and Stevens, 1990).

magnetic field applied along the z axis of a coordinate system, so the Hamiltonian for the alkali-metal atoms is

$$H_a = A_a \mathbf{I}_a \cdot \mathbf{S} + g_s \mu_B S_z B_0 - \frac{\mu_a}{I_a} I_{az} B_0 . \quad (1)$$

The first term is the hyperfine interaction, while the remaining terms give the interaction of the electron and nuclear moments with the external applied field. In low fields, used for most spin-exchange optical pumping experiments, the hyperfine interaction dominates over the Zeeman interactions, so the eigenstates of H_a are also eigenstates of the total angular momentum $\mathbf{F}=\mathbf{S}+\mathbf{I}_a$ and its projection F_z along the external field. We shall be interested mainly in the observables S_z, I_{az}, and $F_z = S_z + I_{az}$. In general we describe the states of the alkali-metal atoms with a density matrix ρ_a whose diagonal elements give the probability of finding the atom in a given state.

Optical pumping can be quite complex in the most general case, especially at low gas pressures where the hyperfine structure of the absorption lines is well resolved (Happer, 1972). However, in almost all applications of spin-exchange optical pumping the following simplifying conditions prevail:

(a) Circularly polarized light is used, resonant with the transition from the $^2S_{1/2}$ ground state of the alkali-metal atom to the lowest $^2P_{1/2}$ excited state.

(b) Pressure broadening of the absorption line makes the alkali-metal hyperfine structure unresolved. For most applications of spin-exchange optical pumping the total noble-gas and nitrogen densities exceed one amagat,[2] giving absorption linewidths of typically 30 GHz or more. For comparison, the largest alkali-metal ground-state hyperfine interval, that of ^{133}Cs, is only 9 GHz.

(c) The quenching gas eliminates radiation trapping as a source of relaxation. This requires N_2 densities of 0.1 amagat or more (Happer, 1972).

(d) As a result of (b) and (c), the nuclear-spin polarization of the atom is conserved in the time interval between excitation by a pumping photon and deexcitation by a quenching collision (Bhaskar *et al.*, 1981).

Under these assumptions, the light spin-polarizes the alkali-metal electrons as shown in Fig. 3. Left-circularly polarized resonance light excites atoms from the spin-down ($m_S=-1/2$) sublevel of the $^2S_{1/2}$ state into the spin-up sublevel ($m_J=1/2$) of the $^2P_{1/2}$ state. Collisions with noble-gas atoms rapidly equalize the sublevel populations of the excited state. Then quenching collisions with N_2 molecules repopulate both ground-state sublevels with nearly equal probability. Since the atoms have $-1/2$ units of electron-spin angular momentum before absorbing the photons and 0 units of electron-spin angular momentum after being quenched from the excited state, on the average each absorbed photon deposits 1/2 unit of spin angular momentum in the vapor, the remainder being lost to translational motion.

The mean photon absorption rate per atom is

$$\langle \delta\Gamma \rangle = (1 - 2\langle S_z \rangle) R_p \quad (2)$$

where R_p, the absorption rate for unpolarized atoms, depends on the spectral profiles of the light and the transition line shape. In practice, both $\langle S_z \rangle$ and R_p are functions of position in the pumping cell. Since each photon adds on the average $\hbar/2$ of angular momentum, the total alkali-metal atomic spin $\langle F_z \rangle$ grows with time as

$$\frac{d\langle F_z \rangle}{dt} = R_p \left(\frac{1}{2} - \langle S_z \rangle \right). \quad (3)$$

B. Collisions between alkali-metal atoms

Spin-exchange collisions between pairs of optically pumped alkali-metal atoms strongly affect the optical

[2]The density of an ideal gas at STP is 1 amagat $= 2.69\times10^{19}\,\mathrm{cm}^{-3}$.

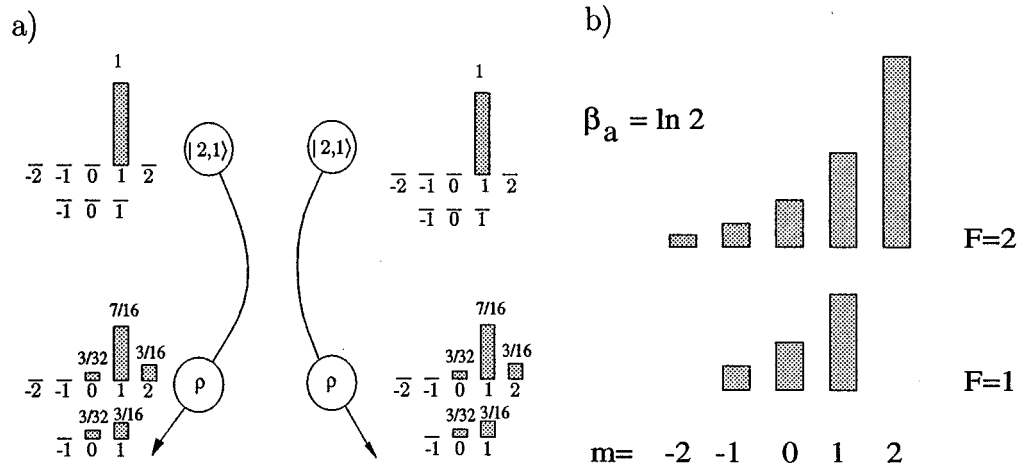

FIG. 5. Alkali metal spin exchange. (a) Example of a spin-exchange collision between two alkali-metal atoms. The total spin of the alkali-metal atoms is rigorously conserved, but the level populations are redistributed by the collisions. (b) Spin-temperature distribution of the spin sublevels, arrived at after many spin-exchange collisions.

pumping process by transferring polarization between the electron spin and the nuclear spin. The alkali-metal-dimer interaction potential, sketched in Fig. 4, has singlet and triplet components. The large splitting of the singlet and triplet potentials causes the electron spins to rotate about each other many times during a single collision. The spin-exchange cross sections are therefore quite large, typically 2×10^{-14} cm^2. This efficient process was first identified by Purcell and Field (1956) to explain the intensity of the 21-cm line radiation in radio astronomy.

Spin-exchange collisions conserve the total spin angular momentum of the colliding atoms, but redistribute the angular momentum between the ground-state sublevels [Fig. 5(a)]. During a spin-exchange collision the hyperfine interaction has little effect, but between collisions it transfers angular momentum internally between the nuclear and electron spins of each alkali-metal atom. Successive collisions like those of Fig. 5(a) lead to the "spin-temperature" distribution (Anderson *et al.*, 1960) illustrated in Fig. 5(b):

$$\rho_a = \frac{e^{\beta_a S_z}}{Z(S,\beta_a)} \frac{e^{\beta_a I_{az}}}{Z(I_a,\beta_a)}. \tag{4}$$

The spin partition function for arbitrary spin K is

$$Z(K,\beta) = \frac{\sinh[\beta(K+1/2)]}{\sinh[\beta/2]}. \tag{5}$$

The spin-temperature parameter β uniquely determines the population distribution for the spin sublevels, so all observables can be expressed in terms of β. In particular, the mean value of K_z is

$$\langle K_z\rangle = \frac{\epsilon(K,\beta)}{2}\tanh\frac{\beta}{2}, \tag{6}$$

where

$$\epsilon(K,\beta) = 2\langle K(K+1) - K_z^2\rangle \tag{7}$$

is called the paramagnetic coefficient.[3] The rate at which the system approaches the spin-temperature distribution depends on the magnetic-field strength (Walker and Anderson, 1993a, 1993b).

Under the conditions of spin-exchange optical pumping, the rate of electron-spin exchange collisions is typically between 10^4 and 10^6 sec^{-1}, which is much greater than other collisional relaxation rates and comparable to or greater than R_p, so the alkali-metal atoms are well described by the spin-temperature distribution. The spin parameter β_a depends on position in the vapor because of spatial variation of pumping light intensity, and β_a may also change with time as the atomic-spin polarization evolves under the influence of optical pumping and relaxation mechanisms. Even when the rate of spin-exchange collisions is small compared to the optical pumping rate, the equilibrium state of the atoms will be well-described by a spin-temperature if the conditions (a)–(c) prevail and if the collisions are of sufficiently short duration that the resulting spin relaxation is well described as "electron randomization."

C. Light propagation

Light radiated by the alkali-metal atoms is nearly unpolarized and can be reabsorbed by the Rb atoms, thereby optically *depumping* the atoms. High Rb vapor pressures are necessary for spin-exchange optical pumping experiments, in order to keep spin-exchange rates large enough to attain high polarizations. Thus the cell is usually many optical depths thick, and a single photon can be scattered several times and thus depolarize sev-

[3]Explicitly, $\epsilon(K,\beta) = (2K+1)\coth(\beta/2)\coth(\beta[K+1/2]) - \coth^2(\beta/2)$. This decreases from $4K(K+1)/3$ at small polarization ($\beta\ll1$) to $2K$ for large polarization ($\beta\gg1$); for $K = 1/2$, $\epsilon(1/2,\beta)=1$.

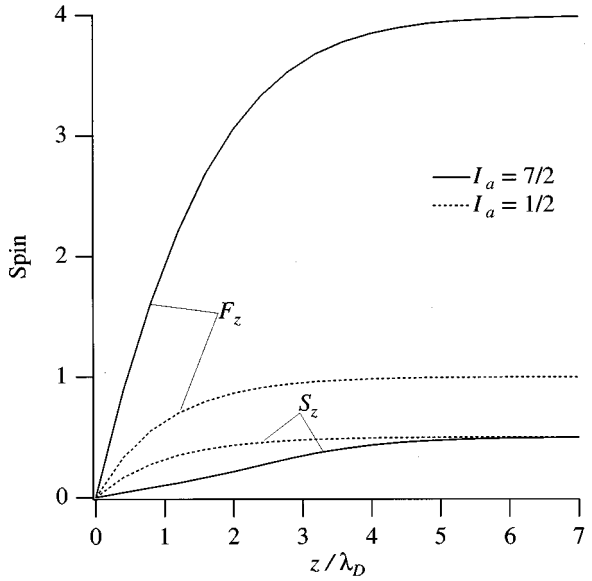

FIG. 6. Polarization as a function of position near the cell wall, where diffusion losses reduce the polarization of the alkali-metal atoms. For $I_a > 1/2$, S_z increases more slowly than F_z because at low polarizations the angular momentum is primarily contained in the nuclear spin.

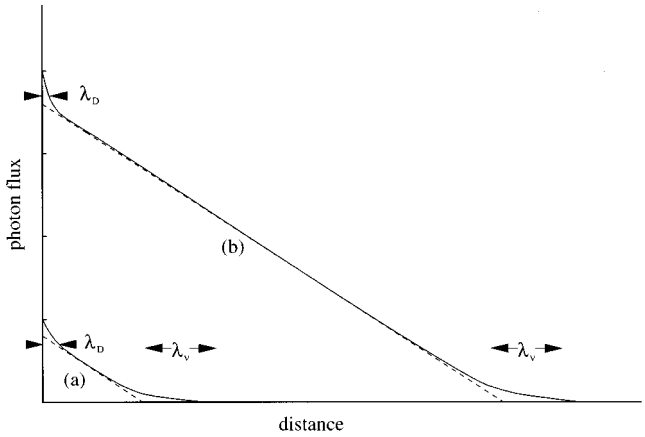

FIG. 7. Attenuation of light as a function of distance through the cell, for (a) low and (b) high incident intensities. λ_ν is the attenuation length for unpolarized atoms.

eral atoms before escaping from the cell (Tupa *et al.*, 1986, 1987). The N_2 quenching gas removes this damaging depolarization mechanism so that intense circularly polarized laser light can still penetrate and illuminate most of the optically thick cell (Bhaskar *et al.*, 1979), as indicated in Fig. 2. In the illuminated part of the cell the spin polarization is nearly 100%. In the dark volume where little light penetrates, the spin polarization is nearly zero. The boundary between the illuminated and dark volumes of the cell is about one optical depth thick. In a well-designed system, matching of the gas composition, the cell temperature, and the spatial profile of the laser intensity allows most of the cell to be illuminated.

Diffusion losses are negligible within the bulk of the cell at the high pressures of these experiments, but diffusion does produce a thin layer near the cell walls where the polarization drops from nearly 100% to zero. The walls are usually bare glass or are coated with various silicone derivatives. The residence time of an adsorbed alkali-metal atom on such a wall is sufficiently long that interactions at the wall completely depolarize both electron and nuclear spins. Thus at the walls $\langle F_z \rangle = 0$, while far away from the wall $\langle F_z \rangle \approx I + 1/2$. In steady-state, optical pumping [Eq. (3)] balances the diffusion losses, so near the cell walls

$$-D_a \frac{d^2\langle F_z \rangle}{dz^2} = R_p \left(\frac{1}{2} - \langle S_z \rangle \right), \tag{8}$$

where D_a is the alkali-metal atom diffusion coefficient. Assuming spin-temperature equilibrium, Fig. 6 shows a numerical integration of Eq. (8). Defining a diffusion length $\lambda_D = \sqrt{2 D_a / R_p}$, we see that S_z is very close to the bulk value within a few diffusion lengths.

The diffusing alkali-metal atoms (density n_a) carry a spin flux

$$j_a = -n_a D_a \frac{\partial}{\partial z} \langle F_z \rangle \approx \frac{1}{2} n_a \sqrt{R_p D_a (2I_a + 1)} \tag{9}$$

to the wall of the cell through which the pumping light enters. The diffusion skin thus attenuates the photon flux by an amount $\Delta J = 2 j_a$. For efficient spin-exchange optical pumping, this flux must be much smaller than the flux $J(0)$ incident on the cell. In spin-exchange pumping of ^{3}He, small alkali-metal/He spin-exchange cross sections necessitate high alkali-metal number densities, possibly violating the condition of negligible spin flux to the wall. Tuning the laser somewhat off resonance to decrease the absorption cross section σ minimizes wall losses while permitting absorption of most of the pumping light (Wagshul and Chupp, 1994; Larson *et al.*, 1991).

Inside the bulk of the cell, absorption by the nearly fully polarized alkali-metal atoms attenuates the laser beam:

$$\frac{dJ}{dz} = -n_a \langle \delta\Gamma \rangle = -n_a (1 - 2\langle S_z \rangle) R_p \,. \tag{10}$$

Collisional spin relaxation and spin exchange make the factor $1 - 2\langle S_z \rangle \approx \bar{\Gamma} / R_p$, where $\bar{\Gamma}$ is the alkali-metal relaxation rate. For pumping light with a much narrower spectral width than that of the optical absorption cross section, $R_p \propto J$, giving

$$J(z) = J(0) - \Delta J - \bar{\Gamma}\, n_a z. \tag{11}$$

This linear attenuation changes to exponential attenuation when the photon flux cannot maintain high spin polarization of the alkali-metal atoms, that is, when $J \leq \bar{\Gamma} / \sigma$ (see Fig. 7).

For broadband pumping sources like diode laser arrays, no well-defined mean free path for the pumping photons exists, so the division of the absorption cell into illuminated regions with high spin polarization of the alkali-metal atoms and dark regions with negligible spin

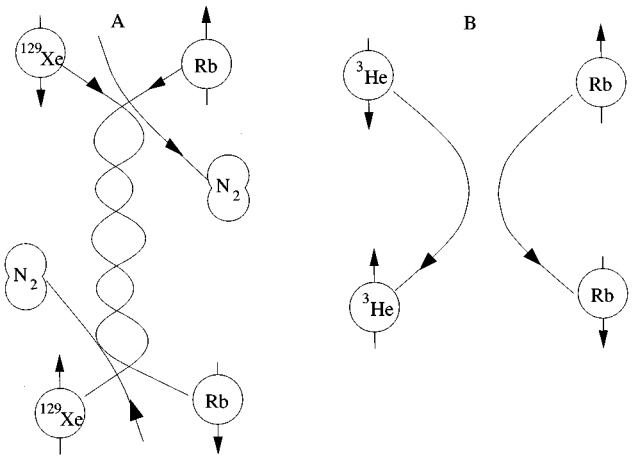

FIG. 8. Polarization transfer processes. (a) Formation and breakup of an alkali-metal/noble-gas van der Waals molecule. (b) Binary collision between an alkali-metal atom and a noble-gas atom.

polarization is blurred. The broad laser linewidth wastes photons, since photons with frequencies too far from the peak optical absorption frequency pass through the cell unattenuated. However, this waste is more than compensated for by the cost savings of inexpensive diode laser arrays as compared to Ti:Sapphire lasers or dye lasers.

IV. SPIN-EXCHANGE

The key process in spin-exchange optical pumping is collisional transfer of polarization between optically pumped alkali-metal atoms and the nuclei of the noble-gas atoms. As indicated in Fig. 8, the transfer of angular momentum occurs either while the atoms are bound in van der Waals molecules or in simple binary collisions between the atoms. For ^{3}He, binary collisions dominate the spin relaxation, and the contribution from van der Waals molecules is negligible. The time for a binary collision ($\sim 10^{-12}$ sec) is so short that the collision can induce both $\Delta F=\pm 1$ and $\Delta F=0$ transitions between the hyperfine sublevels of the alkali-metal atom. For heavier noble gases like ^{129}Xe at total gas pressures of a few tens of Torr, the contributions of van der Waals molecules to the spin relaxation can greatly exceed the contribution of binary collisions. At such low pressures, the collisionally limited lifetime of the van der Waals molecules is long enough ($\geqslant 10^{-9}$ sec) that the total spin angular momentum $F=I_a\pm 1/2$ of the alkali-metal atoms is a good quantum number and the molecules induce relaxation through $\Delta F=0$ transitions. A magnetic field of a few hundred Gauss is sufficient to suppress the relaxation due to van der Waals molecules at these low pressures (Happer *et al.*, 1984). At the multiatmosphere pressures of interest for practical spin-exchange optical pumping, the collisionally limited lifetimes of the van der Waals molecules are so short that their contribution to the relaxation are small compared to that of binary collisions. Most of the residual molecular contribution has the same selection rules as binary collisions—that is, both $\Delta F=0$ and $\Delta F=\pm 1$ transitions are permitted, so the resulting relaxation is nearly indistinguishable from that due to binary collisions. Since we are interested in spin exchange at high gas pressures, we shall henceforth treat the relaxation as if it were all due to binary collisions.

Spin-dependent interactions, denoted $V_1(\mathbf{R})$, produce the spin transfer and relaxation in collisions. For spin-exchange optical pumping, evidence suggests that the spin-rotation interaction between $\mathbf{S}$ and the rotational angular momentum $\mathbf{N}$ and the isotropic hyperfine interaction between $\mathbf{S}$ and the noble-gas nuclear spin $\mathbf{I}_b$ dominate the spin-exchange process:

$$V_1(\mathbf{R})=\gamma(R)\mathbf{N}\cdot\mathbf{S}+A_b(R)\mathbf{I}_b\cdot\mathbf{S}. \tag{12}$$

We discuss these interactions in some detail in Sec. V, but, simply stated, the spin-rotation interaction arises from magnetic fields produced by the relative motion of the charges of the colliding atoms, while the isotropic hyperfine interaction arises from the magnetic field inside the nucleus of the noble-gas atom. V_1 depends strongly on interatomic separation $\mathbf{R}$.

A. Rate equations

The spin-dependent interaction [Eq. (12)] causes transitions between various spin states. The spin-rotation interaction produces relaxation of the alkali-metal electron spins, while the isotropic hyperfine interaction transfers angular momentum back and forth between the alkali-metal electron spins and the noble-gas nuclear spins. In the spin-temperature limit for the alkali-metal atoms, the following two rate equations describe the evolution of angular momentum as a result of collisions between the alkali-metal atoms and the noble-gas atoms under the influence of V_1:

$$\frac{d\langle F_z\rangle}{dt}=-\Gamma_a(\gamma)\langle S_z\rangle-\Gamma_a(A_b)[\epsilon(I_b,\beta_b)\langle S_z\rangle-\langle I_{bz}\rangle] \tag{13}$$

$$\frac{d\langle I_{bz}\rangle}{dt}=\Gamma_b(A_b)[\epsilon(I_b,\beta_b)\langle S_z\rangle-\langle I_{bz}\rangle]. \tag{14}$$

Detailed balance requires that $n_b\Gamma_b(A_b)=n_a\Gamma_a(A_b)$, where n_k is the density of species k. For the important noble gases ^{3}He and ^{129}Xe with $I_b=1/2$, Eq. (14) simplifies to

$$\frac{d\langle I_{bz}\rangle}{dt}=-\Gamma_b(A_b)[\langle I_{bz}\rangle-\langle S_z\rangle]. \tag{15}$$

Thus, in steady-state, if all other relaxation mechanisms are neglected, the noble-gas nuclear-spin polarization equilibrates to the same value as the alkali-metal electron-spin polarization.

The characteristic rates Γ may be estimated from time-dependent perturbation theory (Walker, 1989). For example, given $A_b(R)$ (Sec. V.B), the spin-exchange rate is

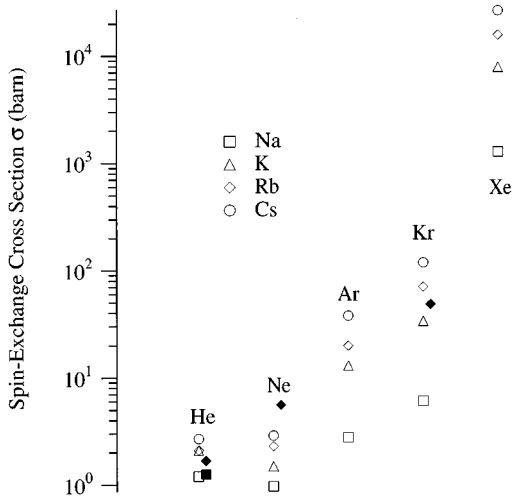

FIG. 9. Spin-exchange cross sections for alkali-metal/noble-gas atom pairs: open symbols, theoretical estimates (Walker, 1989); filled symbols, measurements for Na-He (Soboll, 1972), Rb-He (Coulter, 1989), Rb-Ne (Chupp and Coulter, 1985), and Rb-Kr (Schaefer *et al.*, 1990).

$$\Gamma_b(A_b)=n_a\frac{\pi}{2}\int_0^\infty dbb\int_0^\infty d^3\mathbf{w}f(\mathbf{w})w \times\left|\int_{-\infty}^{\infty}dtA_b(R(t))/\hbar\right|^2, \tag{16}$$

which is an average over the impact parameter b, the velocity distribution $f(\mathbf{w})$, and the classical collision trajectory $R(t)$. An order-of-magnitude estimate is

$$\Gamma_b(A_b)\approx n_a\bar{w}\,\pi R_0^2\frac{A_b(R_0)^2\tau^2}{4\hbar^2}, \tag{17}$$

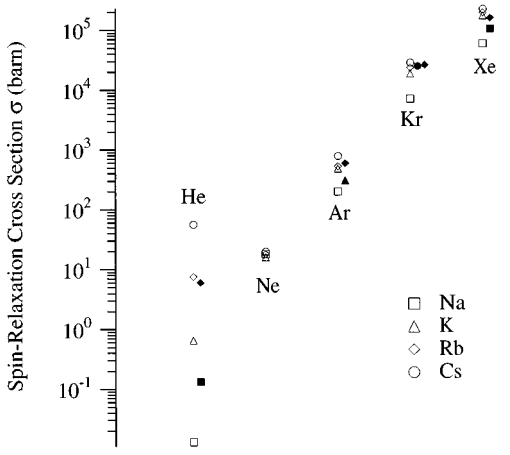

FIG. 10. Spin-relaxation cross sections for alkali-metal/noble-gas atom pairs: open symbols, theoretical estimates (Walker, 1989; Walker *et al.*, 1995); filled symbols, measurements for Na-He (Soboll, 1972), Rb-He (Wagshul and Chupp, 1994), K-Ar (Martin and Anderson, 1995), Rb-Ar,Kr,Xe (Bouchiat *et al.*, 1972), Cs-Kr (Beverini *et al.*, 1973), and Na-Xe (Bhaskar, Hou, Ligare, Suleman, and Happer, 1980).

where R_0 is the distance of closest approach, $\bar{w}$ is the thermal speed, and τ is the collision time. Spin-exchange and relaxation cross sections obtained from the rates using the relation $\Gamma=n\sigma\bar{w}$ are shown in Figs. 9 and 10. These figures show that, for most atom pairs, the spin-relaxation cross sections exceed the spin-exchange cross sections.

B. Photon efficiency

The efficiency of transfer of angular momentum in the spin-exchange process is critical for applications, such as magnetic resonance imaging and polarized targets, that require large numbers of highly polarized noble-gas nuclei. The spin-rotation interaction represents a fundamental limit on the efficiency, but other relaxation mechanisms contribute as well. As pointed out above (Sec. III.C), in well-optimized systems, relaxation in the bulk dominates over spin relaxation of the alkali-metal atoms at the walls. Then bulk relaxation mechanisms limit the photon-to-polarization conversion efficiency.

For small noble-gas polarizations, the angular momentum of the noble-gas nuclei increases at a rate found from Eq. (14):

$$n_bV\frac{d}{dt}\langle I_{bz}\rangle=n_bV\Gamma_b(A_b)\epsilon(I_b,0)\langle S_z\rangle \tag{18}$$

where V is the cell volume, assumed to be fully illuminated. Equations (3) and (13) give the rate at which photons are deposited in the cell as

$$n_aVR_p(1-2\langle S_z\rangle)=2n_aV[\bar{\Gamma}+\Gamma_a(A_b)\epsilon(I_b,0)]\langle S_z\rangle, \tag{19}$$

where $\bar{\Gamma}$ includes relaxation arising from the spin-rotation interaction in collisions with noble-gas atoms and other processes such as spin relaxation in collisions between alkali-metal atoms or alkali-metal–N_2 collisions.

The ratio of Eq. (18) to Eq. (19) determines the transfer efficiency (Bhaskar, Happer, and McClelland, 1982):

$$\eta=\frac{\Gamma_a(A_b)\epsilon(I_b,0)}{2[\bar{\Gamma}+\Gamma_a(A_b)\epsilon(I_b,0)]}. \tag{20}$$

Estimates of the fundamental limiting efficiencies, where $\bar{\Gamma}=\Gamma_a(\gamma)$, range from 0.04 for Rb-Xe to 0.38 for K-He.

V. SPIN-DEPENDENT INTERACTIONS

In this section we describe the current understanding of the physical origins of the spin-dependent forces that are so important for spin-exchange optical pumping. An alkali-metal atom and a noble-gas atom interact via both a large spin-independent interaction $V_0(R)$ and the much smaller, spin-dependent part $V_1(R)$. V_0 can be used to calculate distorted partial waves for subsequent distorted-wave Born approximations of the spin-dependent effects of V_1 (Newbury, Barton, Bogorad, *et al.*, 1993). Equivalently, at the high temperatures of interest, V_0 determines classical collision trajectories,

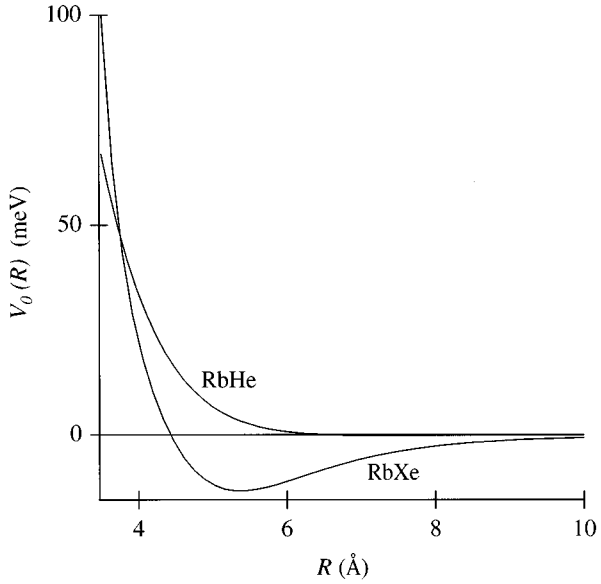

FIG. 11. Spin-independent interaction potentials V_0 between noble-gas and alkali-metal atoms, as calculated by Pascale (1983) and Pascale and Vandeplanque (1974).

along which V_1 acts as a small perturbation (Walker, 1989). The best $V_0(R)$ available use pseudopotential methods constrained by scattering experiments (Buck and Pauly, 1968; Pascale and Vandeplanque, 1974; Pascale, 1983), with examples shown in Fig. 11.

A. Wave functions

Understanding the small spin-dependent interactions requires realistic wave functions for the valence electron in the presence of the noble-gas atom. In principle, these wave functions could be supplied by *ab initio* theory, but such wave functions have been calculated for only a few cases, making it necessary to develop other methods. These methods have generally been quite successful at predicting the strengths of the various interactions and often have simple physical interpretations.

The spin-dependent phenomena generally arise from the electric and magnetic fields generated well inside the cores of either the alkali-metal atom or the noble-gas atom. It is convenient to split the electron wave function ψ into separate parts. Inside each core, the wave function is represented as

$$\psi_k(\mathbf{r}_k)=\phi_0(\mathbf{r}_k)+\sum_i c_{ki}\phi_{ki}(\mathbf{r}_k), \tag{21}$$

where ϕ_0 is the ground-state wave function of the alkali-metal electron in the absence of the noble-gas atom, and the sum extends over the excited orbitals of the alkali-metal atom for $k=a$, and over the occupied core orbitals of the noble-gas atom for $k=b$. Figure 12 shows the geometry.

The free-atom orbitals have the form

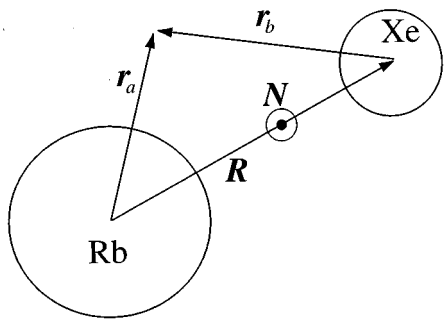

FIG. 12. Geometry used for description of the valence-electron wave function in the presence of a noble-gas atom. The rotational angular momentum of the atom pair is labeled **N**.

$$\phi_{ki}\equiv\phi_{knlm}(\mathbf{r}_k)=\frac{1}{r_k}P_{knlm}(r_k)Y_{lm}(\theta_k,\phi_k), \tag{22}$$

where $P_{knlm}(r_k)$ is a radial wave function of the displacement r_k of the valence electron from the nucleus of the atom k, and $Y_{lm}(\theta_k,\phi_k)$ is a spherical harmonic of the angular coordinates θ_k, ϕ_k. Convenient radial wave functions for core orbitals are available in tabular form (Clementi and Roetti, 1974; McLean and McLean, 1981).

The mixing coefficients c_{ai} inside the alkali-metal core can be estimated using the Fermi pseudopotential (Fermi, 1934; Roueff, 1970),

$$V_F(\mathbf{R})=\frac{2\pi\hbar^2 a}{m}\delta(\mathbf{r}_a-\mathbf{R}), \tag{23}$$

to describe the effective interaction between the valence electron and the noble-gas atom in terms of the electron mass m and the s wave scattering length a. This was first derived to explain the pressure shift of alkali-metal Rydberg states but has since been used for a variety of problems including neutron scattering (Kittel, 1963) and interactions in degenerate Bose gases (Huang, 1987). Table I gives values for a. First-order perturbation

TABLE I. Some important noble-gas characteristics for spin-exchange optical pumping. S wave scattering lengths (a) for electrons scattering from noble-gas atoms (From O'Malley 1963). Orthogonalized wave values of the enhancement factor η, representing the ratio of the electron wave function at the noble-gas nucleus to that of the wave function in the absence of the noble-gas atom. (From Walker *et al.*, 1987). The factor G is a measure of the strength of the spin-orbit interaction in the core of the noble-gas atom.

Atom	a (Å)	η	G (ev Å^5)
He	0.63	-9.5	0.00093
Ne	0.13	15	0.24
Ar	-0.90	-21	1.9
Kr	-1.96	35	12
Xe	-3.4	-50	39

theory predicts

$$c_{ai} = -\frac{2\pi\hbar^2 a}{m E_{ai}} \phi_{ai}(\mathbf{R})\phi_0(\mathbf{R}), \tag{24}$$

where E_{ai} is the excitation energy of state i. These coefficients allow estimates of the alkali-metal isotropic hyperfine shift, the alkali-metal anisotropic hyperfine interaction, and the contribution to the spin-rotation interaction from the core of the alkali-metal atom. For each of these cases either the s or p states dominate, so, neglecting orbitals of larger l,

$$\psi_a(\mathbf{r}_a) = \phi_0(\mathbf{r}_a) + \sum_n \left[c_{ans}\phi_{ans}(\mathbf{r}_a) + c_{anp}\hat{\mathbf{R}}\cdot\boldsymbol{\phi}_{anp}(\mathbf{R})\right]. \tag{25}$$

Here we use the vector p orbital defined by

$$\begin{aligned}\boldsymbol{\phi}_{knp} &= \phi_{knpx}\hat{\mathbf{x}} + \phi_{knpy}\hat{\mathbf{y}} + \phi_{knpz}\hat{\mathbf{z}} \\ &= \sum_m (-1)^m \phi_{kn1m}\hat{\mathbf{u}}_{-m},\end{aligned} \tag{26}$$

depending on whether Cartesian or spherical basis unit vectors ($\hat{\mathbf{u}}_{\pm1} = \mp(\hat{\mathbf{x}} \pm i\hat{\mathbf{y}})/\sqrt{2}$, $\hat{\mathbf{u}}_0 = \hat{\mathbf{z}}$) are used.

A useful approximation for ψ_b, the wave function inside the noble-gas core, results from orthogonalizing the undistorted wave function ϕ_0 to the occupied core orbitals. The orthogonalized wave (OW) approximation (Wu, Walker, and Happer, 1985) is analogous to the well-established orthogonalized plane-wave approximation in solids (Cohen and Heine, 1961) and gives

$$\begin{aligned}\psi_b(\mathbf{r_b}) &= \phi_0(\mathbf{R}+\mathbf{r_b}) \\ &\quad - \sum_i \phi_{bi}(\mathbf{r}_b)\int d^3\mathbf{r}'_b \phi^*_{bi}(\mathbf{r}'_b)\phi_0(\mathbf{R}+\mathbf{r}'_b).\end{aligned} \tag{27}$$

The sum extends over all occupied core orbitals of the noble-gas atom.

The unperturbed wave function varies slowly over the volume of the noble-gas atom, so we represent it with the first two terms (s wave and p wave) of a Taylor series in $\mathbf{r}_b$. With this simplification, Eq. (27) becomes

$$\begin{aligned}\psi_b(\mathbf{r}_b) &= \phi_0(\mathbf{R})\left[1 - \sum_n Q_{bns}\phi_{bns}(\mathbf{r}_b)\right] \\ &\quad + \nabla\phi_0(\mathbf{R})\cdot\left[\mathbf{r}_b - \hat{\mathbf{R}}\sum_n Q_{bnp}\hat{\mathbf{R}}\cdot\boldsymbol{\phi}_{bnp}(\mathbf{r}_b)\right]\end{aligned} \tag{28}$$

where the s and p orbital moments are

$$Q_{bns} = \int \phi_{bns}(\mathbf{r}_b)d^3\mathbf{r}_b \tag{29}$$

$$Q_{bnp} = \frac{1}{3}\int \mathbf{r}_b\cdot\boldsymbol{\phi}_{bnp}(\mathbf{r}_b)d^3\mathbf{r}_b. \tag{30}$$

The first terms in each bracket of Eq. (28), the incident wave in the scattering picture, are normally much smaller than the others generated by the Coulomb potential of the noble-gas atom. Since the ground-state helium atom has no occupied p orbitals, the OW method fails for the p wave inside the helium atom, so integration of the Schrödinger equation is necessary (Walker *et al.*, 1987). Representative wave functions are shown in Fig. 13.

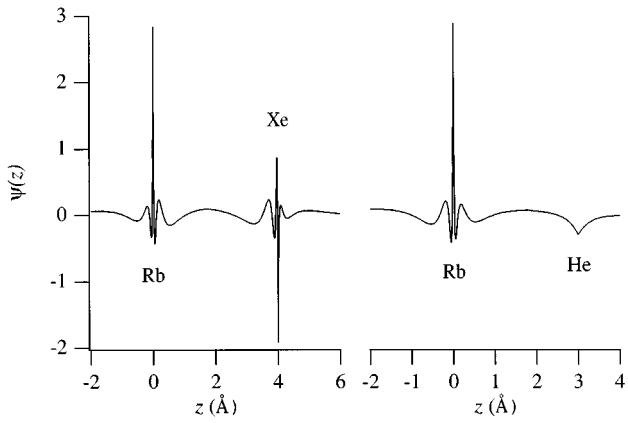

FIG. 13. The valence-electron wave function ψ of Rb-He and Rb-Xe as a function of position along the internuclear axis.

B. Hyperfine interactions

The spin-dependent interaction potential $V_1(R)$, including terms neglected in Eq. (12), can be written as a power series in the rotational angular momentum **N** and the spin operators **S**, $\mathbf{I}_a$, and $\mathbf{I}_b$ of the atomic pair, multiplied by coupling coefficients that are functions of the internuclear separation R:

$$\begin{aligned}V_1(\mathbf{R}) &= \gamma\mathbf{N}\cdot\mathbf{S} + \sum_k A_k(R)\mathbf{I}_k\cdot\mathbf{S} \\ &\quad + \sum_k B_k(R)\mathbf{I}_k\cdot(3\mathbf{RR}-\mathbf{1})\cdot\mathbf{S} \\ &\quad + \sum_k C_k(R)\mathbf{I}_k\cdot(3\mathbf{RR}-\mathbf{1})\cdot\mathbf{I}_k.\end{aligned} \tag{31}$$

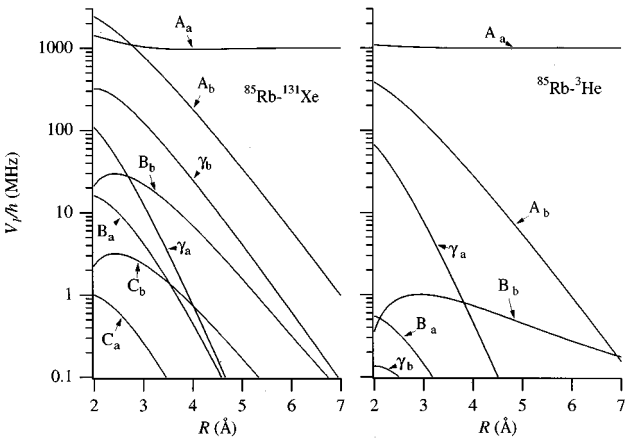

FIG. 14. Spin-dependent interaction strengths as a function of interatomic separation.

Here γ is the coefficient of the spin-rotation interaction, which will be discussed in Sec. V.C. The coupling coefficients for the hyperfine interactions include the following: A_k, for the isotropic magnetic-dipole hyperfine interaction of the nucleus k; B_k, for the anisotropic magnetic-dipole hyperfine interaction; and C_k for the electric quadrupole interaction. Of these coupling coefficients, only A_a remains finite when the atomic pair is well separated. Figure 14 shows representative R dependences of each of the coupling coefficients.

1. Isotropic

The isotropic hyperfine interactions A_a and A_b originate from the Fermi-contact magnetic fields produced by the two nuclei. The term A_b is responsible for spin exchange and is given by (Herman, 1965)

$$A_b(R)=\frac{8\pi g_s\mu_B\mu_b}{3I_b}|\psi_b(0)|^2 =\frac{8\pi g_s\mu_B\mu_b}{3I_b}|\eta\phi_0(R)|^2, \tag{32}$$

where the enhancement factor $\eta=1-\Sigma_n Q_{bns}\phi_{bns}(0)$ represents the ratio of the perturbed wave function at the noble-gas nucleus to what it would be in the absence of the noble-gas atom. Note that η depends only on the properties of the noble-gas atom. Estimates for η are given in Table I, and spin-exchange cross sections in Fig. 9.

The isotropic hyperfine interaction also produces a frequency shift of the magnetic resonance lines of both the alkali-metal and the noble-gas atoms (Schaefer *et al.*, 1989). The frequency shift is characterized by an enhancement factor κ, being the ratio of the shift actually experienced by the alkali-metal electron due to the polarized noble-gas nuclei to that which would be produced by the magnetic field of a noble gas of the same density and polarization contained in a spherical cell. At high pressures the frequency-shift enhancement factor is

$$\kappa_0=\int 4\pi R^2 dR|\eta\phi_0(R)|^2 e^{-V_0(R)/kT}. \tag{33}$$

For a nonspherical cell, long-range dipole-dipole interactions between the polarized nuclei also affect the frequency shift, thereby allowing κ to be measured without accurate density, magnetic field, or polarization measurements. In this way Barton *et al.* (1994) measured κ_0 for Rb-He to $\pm 2.5\%$ accuracy, making measurements of frequency shifts attractive for absolute polarimetry.

The isotropic hyperfine interaction with the alkali-metal nucleus $A_a\mathbf{S}\cdot\mathbf{I_a}$ produces a pressure shift $\delta A_a(R)=A_a(R)-A_a(\infty)$ of the alkali-metal hyperfine splitting. δA results from a change in the unpaired electron density at the alkali-metal nucleus due to the presence of the noble-gas atom, as described by Eqs. (24) and (25). Most experiments on spin-exchange optical pumping make measurements using magnetic resonance spectroscopy of the Zeeman levels of the alkali-metal or noble gas, and are hardly affected by δA_a. However, δA_a causes the pressure shift of the frequency of optically pumped gas-cell clocks, like those used on the GPS satellite system (Riley 1981; Vanier, 1989).

2. Anisotropic

Although quite a bit is known experimentally and theoretically about the isotropic coupling coefficients $A_k(R)$, little consideration has been given to the anisotropic and quadrupole couplings $B_k(R)$ and $C_k(R)$. Based on precise experimental measurements (Childs *et al.*, 1982) of the hyperfine coupling in molecules like CaCl, which is isoelectronic to the van der Waals molecule KAr, Happer *et al.* (1984) argued that only a small percentage of the spin exchange can be due to the anisotropic hyperfine interaction.

The noble-gas anisotropic coupling coefficient from Eq. (31) is

$$B_b(R)=\frac{g_S\mu_B\mu_b}{I_b}\int d^3\mathbf{r}\frac{|\psi(\mathbf{r})|^2}{2r^5}[3\mathbf{r}\cdot\hat{\mathbf{R}}\hat{\mathbf{R}}\cdot\mathbf{r}-r^2]. \tag{34}$$

At large interatomic separations, this interaction gives the dipole-dipole interaction, averaged over the wave function of the alkali-metal atom: $B_b(R)=g_S\mu_B\mu_b/I_bR^3$. For heavy noble gases at smaller interatomic separations, penetration of the alkali-metal electron into the core is the dominant contribution to B_b. Using the wave function of Eq. (28), we find

$$B_b(R)=\frac{2g_S\mu_B\mu_b}{5I_b}|\nabla\phi_0(\mathbf{R})|^2 \times\int_0^\infty\left[\sum_n Q_{bnp}P_{bnp}(r_b)\right]^2\frac{dr_b}{r_b^3}. \tag{35}$$

Numerical estimates are shown in Fig. 14. We see that the anisotropic interaction is probably negligible compared to A_b.

The isotropic magnetic-dipole coupling (proportional to A_b) polarizes the noble-gas nuclei parallel to the electron-spin polarization, while the anisotropic magnetic-dipole coupling polarizes in the opposite direction, to compensate for the excess angular momentum lost to $\langle N_z\rangle$. For example, for the important spin-1/2 noble gases ^{3}He and ^{129}Xe, the rate of change of $\langle I_{bz}\rangle$ including anisotropic coupling is

$$\frac{d\langle I_{bz}\rangle}{dt}=-\Gamma_b(A_b)[\langle I_{bz}\rangle-\langle S_z\rangle]-\Gamma_b(B_b) \times\left[\langle I_{bz}\rangle+\frac{\langle S_z\rangle}{2}\right], \tag{36}$$

where the anisotropic coupling rate is $\Gamma_b(B_b)$. The steady-state solution is

$$\frac{\langle I_{bz}\rangle}{\langle S_z\rangle}=\frac{2\Gamma_b(A_b)-\Gamma_b(B_b)}{2[\Gamma_b(A_b)+\Gamma_b(B_b)]}\approx\frac{A_b^2-B_b^2}{A_b^2+2B_b^2}. \tag{37}$$

Spin-exchange optical pumping produces large polarizations of the noble-gas nuclei only if $A_b^2\gg B_b^2$.

Similar estimates of the strengths of the anisotropic hyperfine interaction in the alkali-metal core, as well as the quadrupole interactions, are shown in Fig. 14. Theoretical estimates indicate these interactions are small compared to A_b and B_b.

C. Spin-rotation interaction

The spin-rotation interaction $\gamma(R)\mathbf{S}\cdot\mathbf{N}$ transfers polarization from the electron spin to the translational degrees of freedom of the atoms, thus limiting the spin-transfer efficiency. The spin-rotation interaction arises from precession of the electron spin about motionally produced magnetic fields inside the core of either the alkali-metal atom or the noble-gas atom. We discuss the two cases separately. For the heavy noble gases, the spin-rotation interaction arises mostly from the noble-gas core, while for He the dominant source is inside the alkali-metal core. Estimates of the two contributions, γ_b and γ_a, respectively, are shown in Fig. 14, while predicted and observed relaxation rates are shown in Fig. 10.

1. Alkali-metal core

The spin-rotation interaction $\gamma\mathbf{S}\cdot\mathbf{N}$ is inherently nonadiabatic in origin. The pair of atoms rotate about each other at a frequency

$$\boldsymbol{\omega}=\frac{\hbar\mathbf{N}}{MR^2}, \tag{38}$$

where M is the reduced mass. To account for this rotation, it is useful to transform to a rotating coordinate system (Van Vleck, 1951), in which the electron experiences a Coriolis interaction,

$$V_\omega=-\hbar\boldsymbol{\omega}\cdot\mathbf{L}. \tag{39}$$

Since this interaction involves the angular momentum $\mathbf{L}$ of the electron, it would vanish to first order were it not for the small admixture of p state into the adiabatic wave function [Eq. (25)] caused by the scattering of the valence electron on the noble-gas atom.

When we use first-order perturbation theory, the wave function including the Coriolis interaction becomes

$$\Psi_a(\mathbf{r}_a)=\psi_a(\mathbf{r}_a)-i\sum_n \frac{\hbar^2 c_{anp}}{MR^2E_{anp}}\hat{\mathbf{R}}\times\mathbf{N}\cdot\boldsymbol{\phi}_{anp}. \tag{40}$$

The expectation value of the spin-orbit interaction $V_{SO}=\xi(r_a)\mathbf{S}\cdot\mathbf{L}$ is then, using the identity $\mathbf{LA}\cdot\boldsymbol{\phi}_{np}=i\mathbf{A}\times\boldsymbol{\phi}_{np}$,

$$\begin{aligned}\langle\Psi_a|V_{SO}|\Psi_a\rangle&=\sum_{nn'}\frac{\hbar^2 c_{anp}c_{an'p}}{MR^2}\left(\frac{1}{E_{anp}}+\frac{1}{E_{an'p}}\right)\\&\quad\times\langle\phi_{anp}|\xi(r_a)|\phi_{an'p}\rangle\mathbf{S}\cdot\mathbf{N}\\&=\gamma_a\mathbf{S}\cdot\mathbf{N}.\end{aligned} \tag{41}$$

The dominant contribution to the sum comes from the first excited p state for which the spin-orbit splitting is $E_{SO}=3\langle\phi_p|\xi(r_a)|\phi_p\rangle/2$, which makes

$$\gamma_a(R)=\frac{4\hbar^2E_{SO}}{3E_pM}\frac{c_{ap}^2(R)}{R^2}. \tag{42}$$

This is proportional to the spin-orbit splitting of the alkali-metal atom and therefore decreases strongly from Cs ($E_{SO}=555\ \mathrm{cm}^{-1}$) to Na ($E_{SO}=17\ \mathrm{cm}^{-1}$). In the Fermi approximation, it is proportional to the square of the noble-gas scattering length and is therefore smallest for Ne.

2. Noble-gas core

In order to estimate the spin-rotation coupling that originates in the noble-gas core, we modify the orthogonalized wave approximation of Eq. (27) to account for the transverse motion $\mathbf{w}=\boldsymbol{\omega}\times\mathbf{R}$ of the atoms. The motion adds translational phase factors to the alkali-metal and noble-gas orbitals, changing the wave function to

$$\Psi_b(\mathbf{r_b})=\psi_b(\mathbf{r_b})-i\frac{m}{MR^2}\sum_n Q_{bnp}\phi_0(\mathbf{R})\mathbf{R}\times\mathbf{N}\cdot\boldsymbol{\phi}_{bnp}, \tag{43}$$

which is quite similar in form to Eq. (40).

The expectation value of the spin-orbit interaction gives (Wu *et al.*, 1985)

$$\gamma_b(R)=-\frac{mG}{MR}\frac{d|\phi_0|^2}{dR}, \tag{44}$$

where the parameter

$$G=\frac{1}{2}\left(\frac{\hbar}{mc}\right)^2\int_0^\infty\left[\sum_n Q_{bnp}P_{bnp}(r_b)\right]^2\frac{1}{r_b}\frac{dV}{dr_b}dr_b \tag{45}$$

reflects the strength of the spin-orbit interaction in the noble-gas core. Equation (44) naturally separates into the factor G that depends only on the noble-gas atom and the factor $d|\phi_0|^2/dR$ that depends on the alkali-metal atom. Table I shows estimated values of G, which increase by orders of magnitude from He to Xe due to the increased strength of the spin-orbit interaction and the increased penetration of the valence electron into the noble-gas core for the heavy atoms.

The two formulas, Eqs. (42) and (44), explain the principal features of Fig. 10. For He, G is so small that γ_a is the dominant contribution to γ. The strong scattering-length dependence of γ_a accounts for the large spread of cross sections for different alkali-metal atoms. For Ar, Kr, and Xe, $\gamma_b\gg\gamma_a$, so the dependence on the alkali-metal atom is slight, while the rates vary over orders of magnitude due to the wide range of values of G.

Spin relaxation can also occur in collisions with the nitrogen quenching gas. For Rb-N_2, the cross section has been recently measured to be $1.2\times10^{-22}\ \mathrm{cm}^2$ (Wagshul, 1994), not significantly larger than the spin-rotation-induced cross sections predicted for Rb-Ne from Fig. 10. The coupling of the electron spin to the rotational angular momentum of the N_2 molecule is an additional potential relaxation mechanism, but this has not been studied.

TABLE II. Measured spin destruction cross sections for alkali-metal pairs (Bhaskar *et al.*, 1980; Knize, 1989).

Atom pair	$\sigma(\mathrm{cm}^2)$
Cs-Cs	2.03×10^{-16}
Rb-Rb	1.6×10^{-17}
K-K	2.4×10^{-18}

VI. OTHER RELAXATION PROCESSES

A. Relaxation in alkali-metal collisions

With the high alkali-metal vapor pressures used in spin-exchange experiments, relaxation in collisions between spin-polarized alkali-metal atoms becomes important. The cross sections vary significantly from Cs-Cs to K-K, as shown in Table II. The relaxation is thought to arise from a tensor interaction $B_{SS}(R)\mathbf{S}\cdot(3\mathbf{RR}-\mathbf{1})\cdot\mathbf{S}$, where in this case $\mathbf{S}=\mathbf{S}_1+\mathbf{S}_2$ is the total electronic spin of the colliding alkali-metal pair. The large Cs-Cs cross section requires B_{SS} to be of the order of 1 cm^{-1} at a typical turning point of 5 Å. The origin of this extremely large coupling is not currently understood.

B. ∇B relaxation

For relaxation due to magnetic-field inhomogeneities, two different regimes can be identified (Cates *et al.*, 1988) depending on the parameter $\varphi=\omega\tau_D$, where ω is the Larmor frequency for the nuclei and $\tau_D\approx R^2/D$ is the characteristic diffusion time for a cell of size R. Letting $\mathbf{\Omega}_\perp$ be the Larmor precession frequency due to the transverse portion of the magnetic-field inhomogeneity, at high pressures ($\varphi\gg1$) the relaxation rate for the spin polarization approaches (Schearer and Walters, 1965)

$$\Gamma_{\nabla B}=\frac{|\nabla\mathbf{\Omega}_\perp|^2D}{\omega^2}, \tag{46}$$

which is inversely proportional to the pressure, since the diffusion coefficient is inversely proportional to pressure. This condition is usually well satisfied for spin-exchange optical pumping experiments. At high pressures, the atoms nearly adiabatically follow the local direction of the magnetic field. The correlation time is roughly the mean time $\tau=\lambda/v$ between collisions, and between collisions the atoms see a field rotating at roughly a frequency $\chi\sim v\nabla\Omega_\perp/\omega$. The relaxation rate is therefore approximately $\Gamma_{\nabla B}\sim\chi^2\tau=v\lambda|\nabla\mathbf{\Omega}_\perp|^2/\omega^2$, which corresponds to Eq. (46).

C. Wall relaxation

In spin-exchange optical pumping experiments, the cell walls are normally prepared with sufficient care that the relaxation due to the wall takes at least tens of minutes and can be as long as days. Under these conditions, the noble-gas polarization is essentially uniform throughout the cell, so the very slow loss of spin polarization to the walls can be described by a wall relaxation time T_w. T_w can be expressed in terms of the cell geometry and the probability α of spin destruction in a single wall collision. The spin flux into the cell wall is $j_I=n_b\bar{w}\langle I_{bz}\rangle/4$, so the rate at which spin polarization is lost at the walls is $n_bV/T_w\langle I_{bz}\rangle=\alpha j_IA$, where A is the surface area of the cell. The wall relaxation time is therefore $T_w=4V/\alpha\bar{w}A$. The detailed physical mechanisms of wall relaxation are poorly understood at present.

For the case of ^{129}Xe, silicone coatings are known to extend wall relaxation times substantially, from tens of seconds to tens of minutes (Zeng *et al.*, 1983). Recent work (Driehuys *et al.*, 1995) showed that the relaxation is dominated by absorption of the Xe by the coating for times as long as several microseconds. Spin transfer from the ^{129}Xe to the protons in the coating reduces the spin-relaxation time of the Xe, but under optimum conditions can cause orders-of-magnitude increases in proton polarizations and allow NMR studies of surfaces. For ^{3}He, relaxation times in well-prepared cells can be tens of hours, increasing to over 100 hours for a Cs film surface (Heil *et al.*, 1995).

D. Noble-gas self-relaxation

The three most intensely studied nuclei for spin-exchange optical pumping are ^{3}He, ^{129}Xe, and ^{131}Xe. Gas-phase relaxation due to self-collisions of these atoms is dominated by three different mechanisms, the nuclear magnetic-dipole-magnetic-dipole interaction for ^{3}He, the nuclear spin-rotation interaction for ^{129}Xe, and the electric-quadrupole interaction for ^{131}Xe.

For ^{3}He, the dipole-dipole interaction dominates the bulk relaxation in the gas phase (Mullin *et al.*, 1990; Newbury, Barton, Cates, Happer, and Middleton, 1993). With careful wall preparation, it is possible to achieve samples for which bulk relaxation dominates. At high temperatures, many partial waves contribute to the spin-flip scattering and the relaxation time increases with increasing temperature. At temperatures of a few K, the smaller partial waves dominate and the rate reaches a minimum before increasing again at lower temperatures.

For ^{129}Xe, gas-phase relaxation arises from the spin-rotation interaction in collisions between Xe atoms (Hunt and Carr, 1963; Torrey 1963). The dipole-dipole interaction is negligible. The observed relaxation times are given by $T_1n_b=2\times10^5$ s-amagat and are in good agreement with theory.

For all the stable noble-gas nuclei other than ^{129}Xe and ^{3}He, the electric quadrupole interaction dominates the gas-phase relaxation. During binary collisions, the interaction between the induced electric-field gradients and the nuclear quadrupole moments produce torques on the spins, thus causing relaxation. These interactions are well understood. For ^{131}Xe, for example, the measured rate $T_1n_b=25.3$ s-amagat (Brinkman *et al.*, 1962) is in excellent agreement with theory (Staub, 1956).

VII. SUMMARY

Spin-exchange optical pumping of noble gases like ^{3}He and ^{129}Xe involves a wide range of atomic, molecular, and optical physics. In this review we have focused on the fundamental spin interactions between alkali-metal atoms and noble-gas atoms. The key physics of these interactions is summarized in Fig. 9 and Fig. 10, which show theoretical and experimental cross sections for spin exchange and spin destruction rates. Both cross sections increase rapidly with the atomic number of the noble-gas atom. The cross sections also increase with atomic number of the alkali-metal atom, a dependence which is particularly pronounced in the spin-relaxation cross sections of ^{3}He. Thus, if lasers were equally practical for all D_1 lines (Na—590 nm; K—770 nm; Rb—795 nm; Cs—894 nm), and if one could ignore issues like the need for higher-temperature operation for the lighter alkali atoms and the need to limit the gas pressure to keep the D_1 and D_2 lines well resolved, it would be best to use Na or K for spin-exchange pumping of ^{3}He and best to use Cs or Rb for spin-exchange pumping of ^{129}Xe, since these choices would maximize the spin transfer rates from the alkali-metal atoms to the noble-gas atoms while minimizing the spin destruction rates. Careful, systematic measurements of the spin destruction rates would be most useful to test these predictions. Experimental measurements show that, at very high temperatures, there is a contribution to the electron-spin destruction rate that is proportional to the density of the alkali-metal atoms. If these rates are due to collisions of alkali-metal atoms with each other, there is a serious disagreement with existing theoretical estimates. Further work to resolve this discrepancy is badly needed and of considerable practical importance.

ACKNOWLEDGMENTS

We have benefitted from many helpful discussions with Mr. D. K. Walter. This work was supported by the National Science Foundation (NSF), the David and Lucile Packard Foundation, the US Air Force Office of Scientific Research (AFOSR), and the Defense Advanced Research Project Agency (DARPA).

REFERENCES

Albert, M. S., G. D. Cates, B. Driehuys, W. Happer, C. S. Springer Jr., B. Saam, and A. Wishnia, 1994, Nature **370**, 199.
Anderson, L. W., F. M. Pipkin, and J. C. Baird, 1960, Phys. Rev. Lett. **120**, 1279.
Anthony, P., *et al.* (E124 Collaboration), 1993, Phys. Rev. Lett. **71**, 959.
Barton, A. S., N. R. Newbury, G. D. Cates, B. Driehuys, H. Middleton, and B. Saam, 1994, Phys. Rev. A **49**, 2766.
Beverini, N., P. Violino, and F. Strumia, 1973, Z. Phys. **265**, 189.
Bhaskar, N. D., J. Camparo, W. Happer, and A. Sharma, 1981, Phys. Rev. **23**, 3048.
Bhaskar, N. D., W. Happer, M. Larsson, and X. Zeng, 1983, Phys. Rev. Lett. **50**, 105.
Bhaskar, N. D., W. Happer, and T. McClelland, 1982, Phys. Rev. Lett. **49**, 25.
Bhaskar, N. D., M. Hou, M. Ligare, B. Suleman, and W. Happer, 1980, Phys. Rev. A **22**, 2710.
Bhaskar, N. D., M. Hou, B. Suleman, and W. Happer, 1979, Phys. Rev. Lett. **43**, 519.
Bhaskar, N. D., J. Pietras, J. Camparo, W. Happer, and J. Kiran, 1980, Phys. Rev. Lett. **44**, 930.
Bouchiat, M. A., J. Brossel, and L. C. L. Pottier, 1972, J. Chem. Phys. **56**, 3703.
Brinkman, D., E. Brun, and H. H. Staub, 1962, Helv. Phys. Acta **35**, 431.
Buck, U., and H. Pauly, 1968, Z. Phys. **208**, 390.
Cates, G. D., S. R. Schaefer, and W. Happer, 1988, Phys. Rev. A **37**, 2877.
Childs, W. J., D. R. Cok, and L. S. Goodman, 1982, J. Chem. Phys. **76**, 3993.
Chupp, T. E., and K. P. Coulter, 1985, Phys. Rev. Lett. **55**, 1074.
Chupp, T. E., R. J. Hoare, R. L. Walsworth, and Bo Wu, 1994, Phys. Rev. Lett. **72**, 2363.
Clementi, E., and C. Roetti, 1974, At. Data Nucl. Data Tables **14**, 177.
Cohen, M. H., and V. Heine, 1961, Phys. Rev. **122**, 1821.
Coulter, K. P., 1989, Ph. D. thesis (Princeton University).
Driehuys, B., G. D. Cates, and W. Happer, 1995, Phys. Rev. Lett. **74**, 4943.
Fermi, E., 1934, Nuovo Cimento **11**, 157.
Happer, W., 1972, Rev. Mod. Phys. **44**, 169.
Happer, W., E. Miron, S. Schaefer, D. Schreiber, W. A. van Wijngaarden, and X. Zeng, 1984, Phys. Rev. **29**, 3092.
Heil, W., H. Humblot, E. Otten, M. Schafer, R. Sarkau, and M. Leduc, 1995, Phys. Lett. A **201**, 337.
Herman, R., 1965, Phys. Rev. **137**, 1062A.
Huang, K., 1987, *Statistical Mechanics* (Wiley, New York).
Hunt, E. R., and H. Y. Carr, 1963, Phys. Rev. **130**, 2302.
Kittel, C., 1963, *Quantum Theory of Solids* (Wiley, New York).
Knize, R. J., 1989, Phys. Rev. A **40**, 6219.
Krauss, M., and W. J. Stevens, 1990, J. Chem. Phys. **93**, 4236.
Larson, B., O. Hausser, P. P. J. Delheij, D. M. Whittal, and D. Thiessen, 1991, Phys. Rev. A **44**, 3108.
Martin, C., and L. W. Anderson, 1996, Phys. Rev. A **53**, 921.
McLean, A. D., and R. S. McLean, 1981, At. Data Nucl. Data Tables **26**, 197.
MacFall, J.R., 1996, Radiology **200**, 553.
Middleton, H., R. D. Black, B. Saam, G. D. Cates, G. P. Cofer, R. Guenther, W. Happer, L. W. Hedlund, G. A. Johnson, K. Juvan, and J. Swartz, 1995, Magn. Reson. Med. **33**, 271.
Mullin, W. J., F. Laloë, and M. G. Richards, 1990, J. Low Temp. Phys. **80**, 1.
Newbury, N. R., A. S. Barton, P. Bogorad, G. D. Cates, M. Gatzke, B. Saam, L. Han, R. Holmes, P. A. Souder, J. Xu, and D. Benton, 1991, Phys. Rev. Lett. **67**, 3219.
Newbury, N. R., A. S. Barton, P. Bogorad, G. D. Cates, M. Gatzke, H. Mabuchi, and B. Saam, 1993, Phys. Rev. A **48**, 558.
Newbury, N. R., A. S. Barton, G. D. Cates, W. Happer, and H. Middleton, 1993, Phys. Rev. A **48**, 4411.
O'Malley, T. F., 1963, Phys. Rev. **130**, 1020.
Pascale, J., 1983, Phys. Rev. A **28**, 632.
Pascale, J., and J. Vandeplanque, 1974, J. Chem. Phys. **60**, 2278.
Purcell, E. M., and G. B. Field, 1956, Astrophys. J. **124**, 542.

Raftery, D., H. Long, T. Meersmann, P. J. Granineti, L. Reven, and A. Pines, 1991, Phys. Rev. Lett. **66**, 584.
W. Riley, 1981, in *Proceedings of the 13th Annual Precise Time and Time Interval (PTTI) Applications and Planning Meeting* (Goddard Space Flight Center), 607.
Roueff, E., 1970, Astron. Astrophys. **7**, 4.
Schaefer, S. R., G. D. Cates, T. R. Chien, D. Gonatas, W. Happer, and T. G. Walker, 1989, Phys. Rev. A **39**, 5613.
Schaefer, S. R., G. D. Cates, and W. Happer, 1990, Phys. Rev. A **41**, 6063.
Schearer, L. D. and G. K. Walters, 1965, Phys. Rev. **139**, A1398.
Soboll, H., 1972, Phys. Lett. A **41**, 373.
Staub, H. H., 1956, Helv. Phys. Acta **29**, 246.
Thompson, A. K., A. M. Bernstein, T. E. Chupp, D. J. DeAngelis, G. E. Dodge, G. Dodson, K. A. Dow, M. Farkhondeh, W. Fong, J. Y. Kim, R. A. Loveman, J. M. Richardson, H. Schmieden, D. R. Tieger, T. C. Yates, M. E. Wagshul, and J. D. Zumbro, 1992, Phys. Rev. Lett. **68**, 2901.
Torrey, H. C., 1963, Phys. Rev. **130**, 2306.
Tupa, D., L. W. Anderson, D. L. Huber, and J. E. Lawler, 1986, Phys. Rev. A **33**, 1045.
Tupa, D., L. W. Anderson, 1987, Phys. Rev. A **36**, 2142.
Vanier, J., and C. Audoin, 1989, *The Quantum Physics of Atomic Frequency Standards* (Institute of Physics, Bristol).
Van Vleck, J. H., 1951, Rev. Mod. Phys. **23**, 213.
Wagshul, M. E., and T. E. Chupp, 1989, Phys. Rev. A **40**, 4447.
Wagshul, M. E., and T. E. Chupp, 1994, Phys. Rev. A **49**, 3854.
Walker, T. G., 1989, Phys. Rev. A **40**, 4959.
Walker, T., and L. W. Anderson, 1993, Phys. Rev. Lett. **71**, 2346.
Walker, T., and L. W. Anderson, 1993, Nucl. Instrum. Methods Phys. Res. A **334**, 313.
Walker, T. G., K. Bonin, and W. Happer, 1987, Phys. Rev. A **35**, 3749.
Walker, T. G., J. Thywissen, and W. Happer, 1995, unpublished.
Wu, Z., W. Happer, M. Kitano, and J. Daniels, 1990, Phys. Rev. A **42**, 2774.
Wu, Z., T. G. Walker, and W. Happer, 1985, Phys. Rev. Lett. **54**, 1921.
Zeng, X., E. Miron, W. A. van Wijngaarden, D. Schreiber, and W. Happer, 1983, Phys. Lett. A **96**, 191.